INSTITUTE OF PHYSICS PUBLISHING JOURNAL OF OPTICS A: PURE AND APPLIED OPTICS

J. Opt. A: Pure Appl. Opt. **6** (2004) S142–S150 PII: S1464-4258(04)66828-0

# Sub-Doppler spectroscopy of Rb atoms in a sub-micron vapour cell in the presence of a magnetic field

**David Sarkisyan[1], Aram Papoyan[1], Tigran Varzhapetyan[1], Janis Alnis[2], Kaspars Blush[2] and Marcis Auzinsh[2]**

[1] Institute for Physical Research, NAS of Armenia, Ashtarak-2 378410, Armenia
[2] Department of Physics, University of Latvia, 19 Rainis Boulevard, Riga, LV-1585, Latvia

Received 30 July 2003, accepted for publication 9 January 2004
Published 24 February 2004
Online at stacks.iop.org/JOptA/6/S142 (DOI: 10.1088/1464-4258/6/3/023)

**Abstract**
We report the first sub-Doppler study of the magnetic field dependence of laser-induced fluorescence excitation spectra of alkali atoms making use of an extremely thin vapour cell (thickness $\sim$ 400 nm). This thin cell allows for sub-Doppler resolution without the complexity of atomic beam or laser cooling techniques. This technique is used to study the laser-induced fluorescence excitation spectra of Rb in a 50 G magnetic field. At this field strength the electronic angular momentum **J** and nuclear angular momentum **I** are only partially decoupled. As a result of the mixing of wavefunctions of different hyperfine states, we observe a nonlinear Zeeman effect for each sublevel, a substantial modification of the transition probabilities between different magnetic sublevels, and the appearance of transitions that are strictly forbidden in the absence of the magnetic field. For the case of right- and left-handed circularly polarized laser excitation, the fluorescence spectra differ qualitatively. Well pronounced magnetic field induced circular dichroism is observed. These observations are explained with a standard approach that describes the partial decoupling of **I** and **J** states.

**Keywords:** rubidium vapour, sub-Doppler spectrum, hyperfine transitions, magnetic circular dichroism, polarization

## 1. Introduction

Sub-Doppler probes of atoms and molecules in a thermal gas cell is a well-established subfield of laser spectroscopy. In particular, velocity-selective techniques, such as saturated absorption spectroscopy, polarization spectroscopy, Doppler-free two photon spectroscopy (i.e. velocity cancelling technique) [1, 2], coherent dark state spectroscopy [3] and other techniques can provide linewidths orders of magnitude smaller than the Doppler width.

During the past several years a fundamentally different approach has been developed. This new method is based on the spectroscopy of a diluted atomic vapour in an extremely thin cell. In most of these studies thermal Cs atoms are confined to cells of thickness of 10–1000 $\mu$m. The Cs atoms that are moving parallel to the cell walls are laser excited and fluoresce in much the same way as atoms in a normal vapour cell. Atoms moving perpendicularly to the closely-spaced cell walls are likely to suffer collisions with the wall before they absorb and fluoresce and therefore do not make a significant contribution to the laser-induced fluorescence signal. Thus the spectra obtained is that of atoms that show no first-order Doppler shift. This approach allows for a relatively simple experimental apparatus to provide sub-Doppler resolution [4–10].

It was demonstrated a long time ago in microwave spectroscopy [11], and recently in the optical domain [12–15], that the optimal cell thickness $L$ for atomic line shape narrowing is approximately $\lambda/2$ where $\lambda$ is the wavelength of spectral features to be observed. This fact stimulated us (DS and AP) to develop an extremely thin gas cell of thickness 100–300 nm. As far as we know this is an absolute record. The cell used in the present investigation is at least one order of magnitude thinner than all other cells used in this manner and has allowed the first optical measurement of atoms in a cell which satisfies the condition $L \approx \lambda/2$. These

  

conditions recently allowed the resolution of all hyperfine transitions of the $D_2$ line of Cs atoms [16]. In addition to the Cs study, a naturally occurring isotopic mixture of Rb atoms was introduced to the thin cell. For this case, $^{85}$Rb and $^{87}$Rb hyperfine transitions were well resolved in the first $D_1$ line fluorescence spectrum [16]. In addition to removing Doppler broadening, thin cells provide a second advantage that is not evident in other types of spectroscopy: in an ordinary vapour cell it is extremely easy to reach laser intensities that change the atomic ground state magnetic sublevel population (optical pumping) and to saturate transitions. In ordinary cells optical pumping of atomic states typically occurs at laser radiation intensities of 10–1000 nW cm$^{-2}$, complicating the experimental determination of relative absorption strengths and/or atomic populations. In a thin cell, however, the population of atoms that do not move parallel to the cell walls constantly replenishes the depleted ground-state population, leading to linear laser absorption at laser intensities up to at least 50 mW cm$^{-2}$ [16].

In the present paper we demonstrate that a sub-micron cell not only allows for sub-Doppler atomic spectroscopy, but more sophisticated studies of linear magneto-optical effects as well. Specifically, we use sub-micron cells filled with $^{85}$Rb and $^{87}$Rb to explore circular dichroism induced by an external magnetic field. The effect of magnetic field induced circular dichroism is important for a variety of reasons. For some time there have been attempts to use polarization plane rotation of a laser beam by an atomic or molecular gas to test for CP parity violation caused by interference between the neutral weak and electromagnetic interactions that couple a valence electron to the nucleus [17–20]. Alkali atoms including Cs are considered as a perspective object for such CP parity violation measurements [21]. Simple linear magneto-optical effects caused by stray magnetic fields in general and magnetic field induced circular dichroism in particular can mimic the effect of rotation of the laser beam polarization plane by parity-violating neutral currents. It is therefore essential that the less exotic linear magneto-optical effect be completely understood. In a more practical application, magnetic field induced circular dichroism in alkali atoms has been successfully applied for a diode laser frequency stabilization based on the difference of the absorption of right- and left-hand circularly polarized radiation in atomic vapour placed in a constant magnetic field [22, 23]. This technique was applied to diode lasers in the work of the Joint Institute for Laboratory Astrophysics (JILA) group [24], who coined for this stabilization method the term *dichroic atomic vapour laser lock* (DAVLL).

In general circular dichroism studies in alkali metal vapours have a long history. The first detailed study of magneto-optical rotational effects for closely lying hyperfine levels was performed in connection with the non-conservation of CP parity in bismuth [25, 26]. The work of Roberts *et al* [26] is a combined theoretical and experimental investigation of magneto-optical effects on Doppler broadened transitions. The primary focus of this work is Faraday rotation, but the closely related phenomenon of magnetic field induced circular dichroism is discussed as well. The shift of the energy of magnetic sublevels in the magnetic field is considered and hyperfine level mixing caused by the field is taken into account as well. Doppler broadened optical rotation spectra and, in one experiment, circular dichroism spectra are observed. Typical features of the spectra have widths of the order of a gigahertz. In a more recent paper [27], Doppler broadened magneto-optical rotation spectra in a room-temperature Cs vapour in a magnetic field of the order of 45 G are presented, along with a corresponding theoretical treatment. An interesting result of the theoretical treatment is the fact that even at this relatively weak magnetic field the perturbation of the wavefunction plays an essential role in the Zeeman energy level shift. In a study carried out in Quebec [28], both isotopes of rubidium $^{85}$Rb and $^{87}$Rb as well as Cs atoms are used to study absorption spectra of atoms in presence of a magnetic field. In this study relatively strong magnetic field strengths of 790, 1440 and 2300 G are applied to the gas cell. It is shown that a magnetic field strength exceeding 1000 G is required to observe magnetic structure in the Doppler broadened absorption spectra. At these high field values hyperfine coupling is broken, and nuclear and electronic moments in the atom are decoupled. Studies of linear magneto-optical methods can be carried out also by non-direct methods like selective reflection spectroscopy [29, 30], but these methods will not be discussed in this work.

In the present paper we demonstrate that extremely thin gas cells can be used successfully to study with sub-Doppler resolution magnetic field induced circular dichroism in atoms. We are not aware of any previous experimental study of magnetic field induced circular dichroism that employs a sub-Doppler technique, although a theoretical study of magneto-optical effects on atoms in a thin cell has been carried out previously [13]. Here we observe magnetic field induced circular dichroism. We measure the total fluorescence intensity dependence on the scanned diode laser frequency (laser-induced fluorescence excitation spectra) for both Rb isotopes. Excitation with circularly polarized, as well as linearly polarized, radiation is used. It is demonstrated that the laser-induced fluorescence excitation spectra are qualitatively very different for left- and right-hand circularly polarized radiation. By contrast, the corresponding Doppler broadened spectra change only slightly as the light helicity changes, and this change may be explained with a simple model that ignores the rich physics observed in the sub-Doppler spectra.

The paper is organized as follows. In section 2 the experimental procedure is presented. In section 3 we describe the results obtained for the two naturally occurring Rb isotopes. Section 4 compares the observed spectra with model calculations. In section 5 the results are discussed, and in section 6 conclusions are drawn.

## 2. Experimental set-up

The design of the extremely thin cell (ETC) is presented in figure 1. It is a new modification of sapphire cells developed earlier (see [16] and references therein). The windows of 30 mm diameter and 3 mm thickness are made from very well-polished garnet (YAG) crystal, which is resistant to highly corrosive alkaline vapours. The roughness of the inner surfaces of the YAG windows is $<\lambda/10$. In order to realize a wedged gap between the YAG windows, a 1 mm wide and 10 mm long $Al_2O_3$ strip coating of $\approx$600 nm thickness has been deposited on the surface of one of the YAG windows, near the lower edge. The sapphire side arm with a molybdenum glass termination is

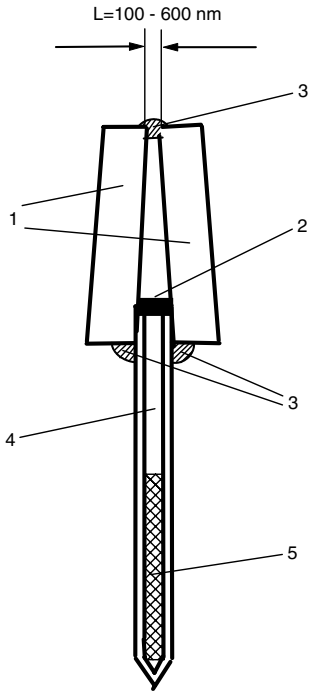


**Figure 1.** The design of the ETC. 1—the windows of the ETC, made from a garnet (YAG) crystal; the thickness is 3 mm, and the diameter is 30 mm. The flatness of both inner surfaces of the YAG windows is less than $\lambda/10$; 2—$\sim$600 nm thick $Al_2O_3$ coating in the shape of a 1 mm wide and 10 mm long strip; 3—the glue; 4—the sapphire side arm with a 'molybdenum glass' termination; 5—column of Rb metal.

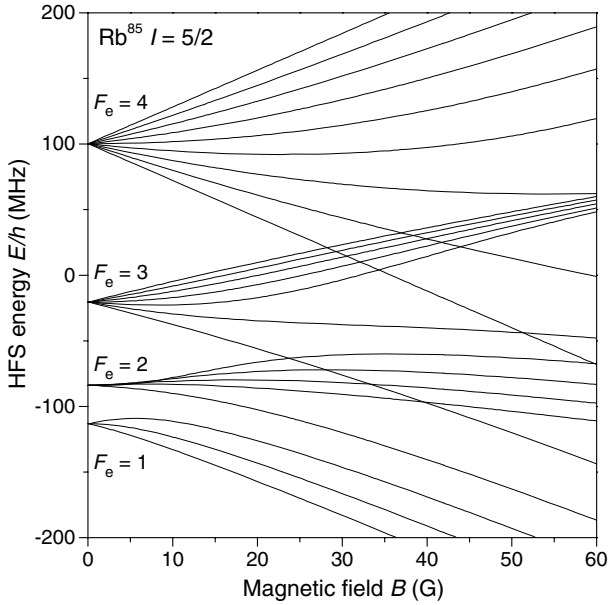


**Figure 2.** Excited-state hyperfine magnetic sublevel splitting for intermediate strength of a magnetic field for $^{85}$Rb isotope.

used for filling the cell with Rb in the same way as for all-glass cells. To attach the side arm, a hole is drilled at the bottom of the YAG windows. Before filling the ETC with a natural mixture of rubidium atoms (72.15% of $^{85}$Rb with nuclear spin $I = 5/2$ and 27.85% of $^{87}$Rb with nuclear spin $I = 3/2$), the cell was carefully out-gassed.

The wedged gap between the windows allows us to exploit a $\sim\lambda/2$ thickness of a vapour layer that is important for having the narrowest sub-Doppler line width [14]. An interferometric mapping of the gap thickness is performed using an He–Ne laser. This measurement shows that the thickness of the gap varies over the range of 100–600 nm. A $\sim$400 nm thickness region of the cell aperture ($\approx\lambda/2$) has been explored in the present experiment.

The upper temperature limit for the ETC is $\sim$400 °C. The ETC operated with a specially designed oven, which has four openings: two for the laser beam transmission and two that allow for fluorescence to be detected simultaneously from two different directions. The density of the Rb atomic vapour is determined by the temperature of the boundary of the Rb metal column inside the side arm (figure 1). The typical value of the metal boundary (side arm) temperature is kept at 120 °C throughout the measurements, while the window temperature is set to a somewhat higher value (140 °C) to prevent Rb condensation. The corresponding number density of Rb atoms is $N_{\mathrm{Rb}} \approx 2 \times 10^{13}$ cm$^{-3}$, and the collisional broadening is $\sim$3 MHz. The Doppler line width in an ordinary cell at this temperature regime is $\approx$600 MHz.

The ETC with Rb atoms is placed in three pairs of mutually perpendicular Helmholtz coils, which cancel the ambient magnetic field and provide a homogeneous magnetic field in an arbitrary direction. The geometry of the experiment is depicted schematically in figure 5. The collimated radiation beam of the cw laser diode ($\lambda = 780.2$ nm, 25 MHz line width, single mode, diameter 3 mm) is directed at normal incidence into the Rb-filled $\sim$400 nm thick region of the ETC. The maximum laser intensity is 50 mW cm$^{-2}$. A Glan–Thomson prism is used to purify the linear radiation polarization of the laser. To produce a circular polarization, a $\lambda/4$ plate is utilized. A photodiode with an aperture of 1 cm$^2$ is placed at 90° to the laser propagation direction to detect the fluorescence signal emerging through one of the two side openings of the cell oven. The photodiode collects emission within a $\sim$0.1 srad solid angle. The signal of the photodiode is amplified and recorded with a storage oscilloscope. The intensity of the fluorescence emission (with no spectral and polarization resolution) from the vapour layer excited by linearly and circularly polarized radiation is recorded versus the laser radiation frequency. To obtain the laser-induced fluorescence excitation spectra, the laser frequency is scanned linearly in a 9 GHz spectral region around the Rb $D_2$ line by means of injection current ramping.

As a result of hyperfine interactions, the ground state level of $^{85}$Rb is split into two components with total angular momentum quantum numbers $F_g = 2$ and 3, and the ground-state level of $^{87}$Rb is split into two components with total angular momentum quantum numbers $F_g = 1$ and 2. The ground state level splitting for $^{85}$Rb and $^{87}$Rb is approximately 3 and 7 GHz, respectively. In contrast, the four excited-state hyperfine components are separated by only several hundred MHz (see figures 2 and 3). Since the separation of the hyperfine sublevels of the $5P_{3/2}$ state with $F_e = 0$–3 for $^{87}$Rb (72–157–267 MHz) and $F_e = 1$–4 for $^{85}$Rb (29–63–121 MHz) is less than the Doppler broadening ($\sim$600 MHz), the $D_2$ spectrum for an ordinary Rb cell consists of only two resolved lines for each Rb isotope: $5S_{1/2}$ ($F = 1$) $\rightarrow$ $5P_{3/2}$ ($F = 0$–2) and $5S_{1/2}$ ($F = 2$) $\rightarrow$ $5P_{3/2}$ ($F = 1$–3) for $^{87}$Rb and $5S_{1/2}$ ($F =$

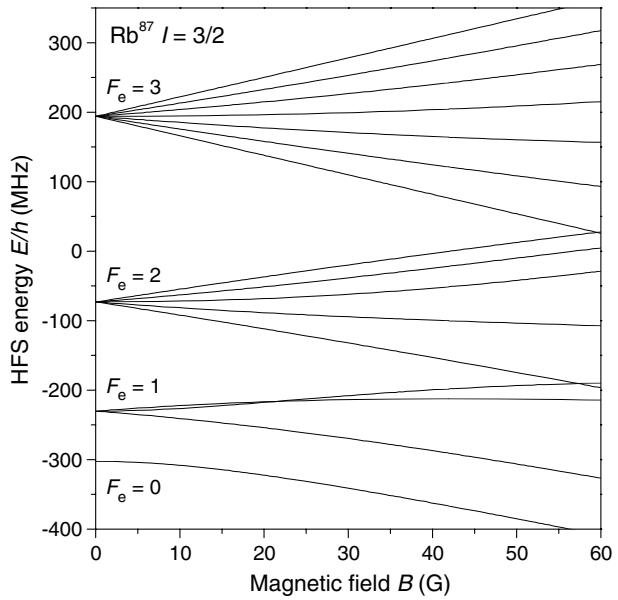


**Figure 3.** Excited-state hyperfine magnetic sublevel splitting for intermediate strength of a magnetic field for the $^{87}$Rb isotope.

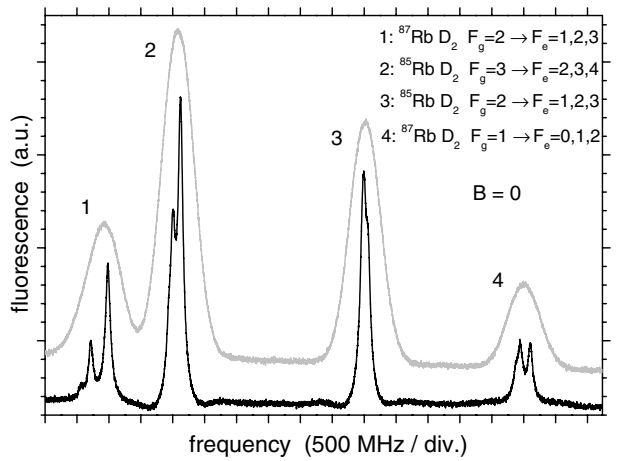


**Figure 4.** Doppler broadened fluorescence spectra (light curve) obtained in an ordinary cell and sub-Doppler spectra obtained in ETC on the $D_2$ line of both Rb isotopes in the absence of the magnetic field.

2) $\rightarrow$ $5P_{3/2}$ ($F$ = 1–3) and $5S_{1/2}$ ($F$ = 3) $\rightarrow$ $5P_{3/2}$ ($F$ = 2–4) for $^{85}$Rb. The total laser-induced fluorescence excitation spectra on a full $D_2$ line scan in the absence of the magnetic field are presented in figure 4. The grey curve shows the Doppler broadened spectrum in an ordinary room-temperature cm-long cell. The black curve shows the same spectrum in an ETC. In the latter, features representing hyperfine levels of the excited state can clearly be seen.

## 3. Measured signals of the magnetic field induced circular dichroism

To explore magneto-optical effects, we register the fluorescence spectra for three different polarizations of laser radiation, namely, left- and right-handed polarization for the case of laser propagation parallel to the magnetic field direction ($\sigma^+$ and $\sigma^-$) and linear polarization along the magnetic field

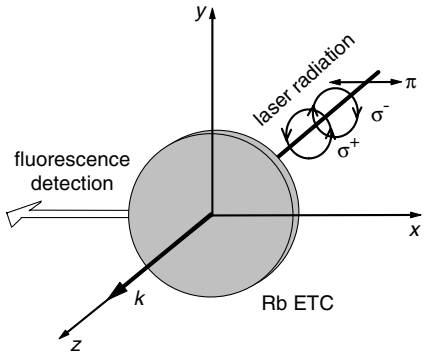


**Figure 5.** The geometrical configuration of the experiment. The magnetic field is applied along the $z$ or $x$ axis.

direction ($\pi$). Our choice of laser radiation polarization and magnetic field direction is determined by the fact that for each of these geometries, only one well defined transition type between magnetic sublevels of ground state $m_{F_g}$ and magnetic sublevels of excited state $m_{F_e}$ can take place. Namely, $\Delta m = m_{F_e} - m_{F_g}$ is equal to +1 for $\sigma^+$ excitation, is equal to $-1$ for $\sigma^-$ excitation, and is equal to 0 for $\pi$ excitation. We record experimental laser-induced fluorescence excitation spectra of Rb atoms at a $B$-field strength of 50 G. This intermediate field strength is chosen so that the Paschen–Back effect is important. At this interesting field strength, the magnetic field starts to decouple the nuclear spin **I** from the electronic angular momentum **J**, but these moments still remain partially coupled. As a rule, at this field strength crossings take place in the magnetically shifted hyperfine levels (see figures 2 and 3).

In figures 6–9 scattered circles depict experimentally obtained signals for the following transitions: $^{85}$Rb, absorption $F_g = 2 \rightarrow F_e = 1, 2, 3, (4)$; $^{85}$Rb, absorption $F_g = 3 \rightarrow F_e = (1), 2, 3, 4$; $^{87}$Rb, absorption $F_g = 1 \rightarrow F_e = 0, 1, 2, (3)$ and $^{87}$Rb, absorption $F_g = 2 \rightarrow F_e = (0), 1, 2, 3$. For reference, in the same figures, experimentally measured fluorescence spectra in the absence of the magnetic field are depicted with lighter colour. We note the observation of transitions that violate the $\Delta F = 0, \pm 1$ selection rule for electric dipole transitions. This selection rule is strictly true only for hyperfine levels in the absence of the magnetic field. As the magnetic field intensity increases from zero, the hyperfine levels mix, and transitions that are forbidden in the absence of the field start to be allowed. The excited-state quantum number for transitions that are not allowed in the absence of a magnetic field are written in parentheses.

From the figures presented it is clearly seen that laser-induced fluorescence excitation spectrum for left- and right-handed excitation are qualitatively different. From simple symmetry considerations, these spectra must coincide in the absence of the magnetic field. In the presence of the field, the helicity of the laser polarization with respect to the field direction starts to play a very important role, and these spectra are very different for all transitions presented. In agreement with nearly linear fluorescence intensity dependence, when the intensity of the diode laser is increased, reported in [16], in the case of Rb the shape of the fluorescence spectrum also does not noticeably depend on the laser radiation intensity, at least in the range of $I_L$ = 1–50 mW cm$^{-2}$. All the spectra presented in the graphs were recorded with $I_L$ = 50 mW cm$^{-2}$.

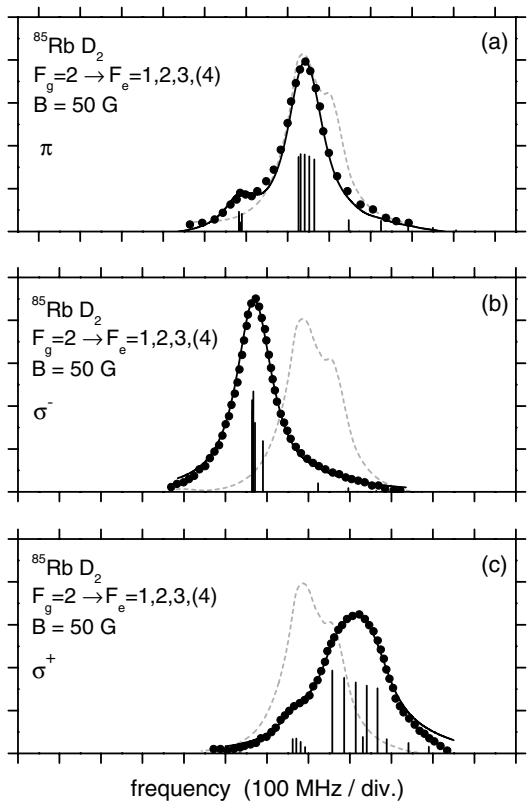


**Figure 6.** Experimental (scattered circles) and simulated (dark line) fluorescence spectra of $^{85}$Rb isotope on transitions $F_g = 2 \rightarrow F_e = 1, 2, 3, (4)$. (a) linearly polarized $\pi$ excitation, (b) circularly polarized $\sigma^-$ excitation, (c) circularly polarized $\sigma^+$ excitation. The respective fluorescence spectra in the absence of the magnetic field are shown with the light lines.

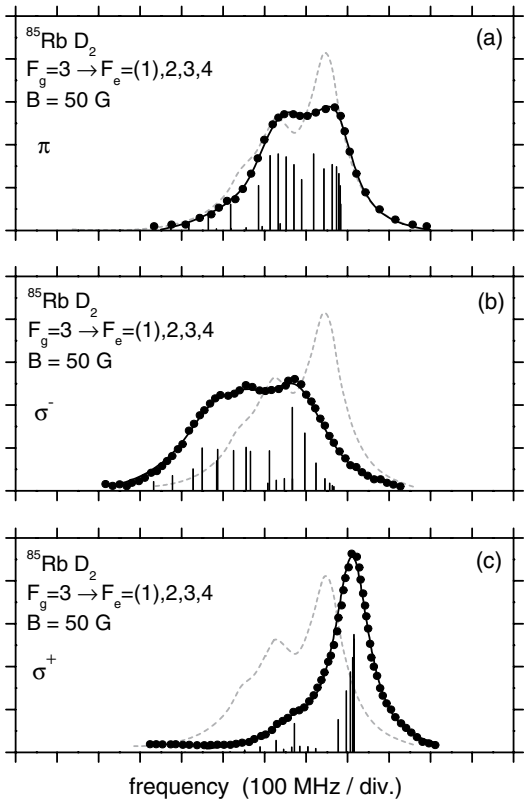


**Figure 7.** Experimental (scattered circles) and simulated (dark line) fluorescence spectra of $^{85}$Rb isotope on transitions $F_g = 3 \rightarrow F_e = (1), 2, 3, 4$. (a) linearly polarized $\pi$ excitation, (b) circularly polarized $\sigma^-$ excitation, (c) circularly polarized $\sigma^+$ excitation. The respective fluorescence spectra in the absence of the magnetic field are shown with the light lines.

It is interesting to compare these spectra for the case of ordinary cells, when only Doppler broadened spectra can be recorded. In figure 10 absorption spectra obtained at room temperature in an ordinary cell containing pure isotopes of Rb atoms are shown, in one case for $^{85}$Rb and in the other case for $^{87}$Rb. Unfortunately, for technical reasons only the absorption and not the laser-induced fluorescence excitation spectra were taken. Nevertheless, in these cells absorption and laser-induced fluorescence excitation spectra should be very similar. We see that in these Doppler broadened spectra, both isotopes lead to spectra that are qualitatively similar for both circularities of laser radiation. Each isotope leads to only one peak for absorption from each of the ground state hyperfine levels. This peak is shifted for two excitation light polarizations on a frequency scale. This peak shifting is the phenomenon that the diode-laser stabilization schemes [22–24] mentioned in the introduction exploit.

As we can see from figures 6–9, the transitions between individual magnetic sublevels $m_{F_g} \rightarrow m_{F_e}$ of the same hyperfine transition $F_g \rightarrow F_e$ are not resolved in the conditions of present experiment. Indeed, in the case of complete resolution, one would expect up to 9 transitions between different magnetic sublevels in the case of circularly polarized excitation for $F_i = 1 \rightarrow F_e = 0, 1, 2, (3)$ (cases (b) and (c) figure 8) and up to 22 magnetic transitions for the case of linearly polarized excitation for $F_i = 3 \rightarrow F_e = (1), 2, 3, 4$ (case (a) figure 7). The results of this experiment can rather be interpreted as $B$-field dependent frequency shifts and variation of probabilities of the $|F_g, m_g\rangle \rightarrow |F_e, m_e\rangle$ hyperfine transitions. In the present experiment an essential limitation for the resolution comes from the width of excitation laser line, which was equal to 25 MHz. This allows us to hope that in future the resolution of sub-Doppler spectroscopy in ETC can be increased and can be close to the homogeneous line width of atomic transitions.

## 4. Laser-induced fluorescence excitation spectra in a magnetic field: signal simulation

As we see from the observed signals, there exists a well pronounced structure in laser-induced fluorescence excitation spectra. This structure changes when the magnetic field is applied. It cannot be observed in Doppler broadened spectra. A similar structure was observed earlier by [28], but only in an extremely strong magnetic field with strength of the order of 1000 G and stronger. At this field strength the electronic angular momentum **J** of an alkali atom is decoupled from the nuclei spin angular momentum **I** and both angular momenta interact with the external field practically independently. In the present study, **J** and **I** are only partially decoupled, and we can observe the Paschen–Back effect.

To simulate the fluorescence spectra of Rb atoms in a magnetic field of intermediate strength, we will use the

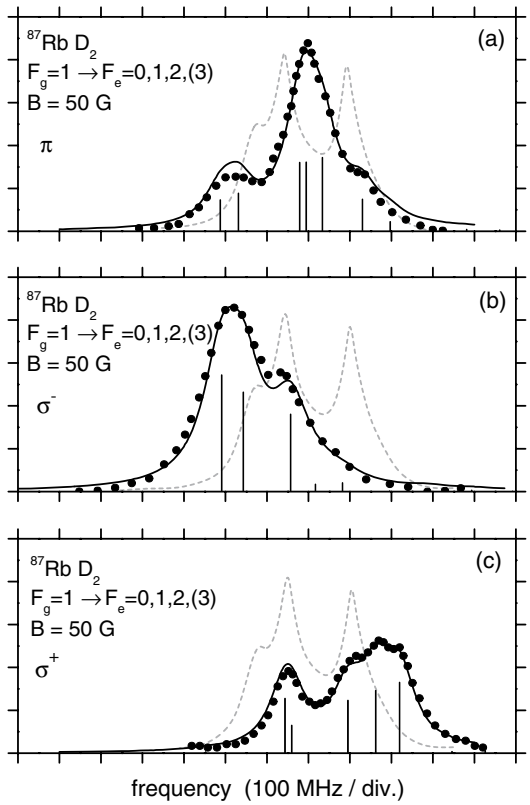


**Figure 8.** Experimental (scattered circles) and simulated (dark line) fluorescence spectra of $^{87}$Rb isotope on transitions $F_g = 1 \rightarrow F_e = 0, 1, 2, (3)$. (a) linearly polarized $\pi$ excitation, (b) circularly polarized $\sigma^-$ excitation, (c) circularly polarized $\sigma^+$ excitation. The respective fluorescence spectra in the absence of the magnetic field are shown with the light lines.

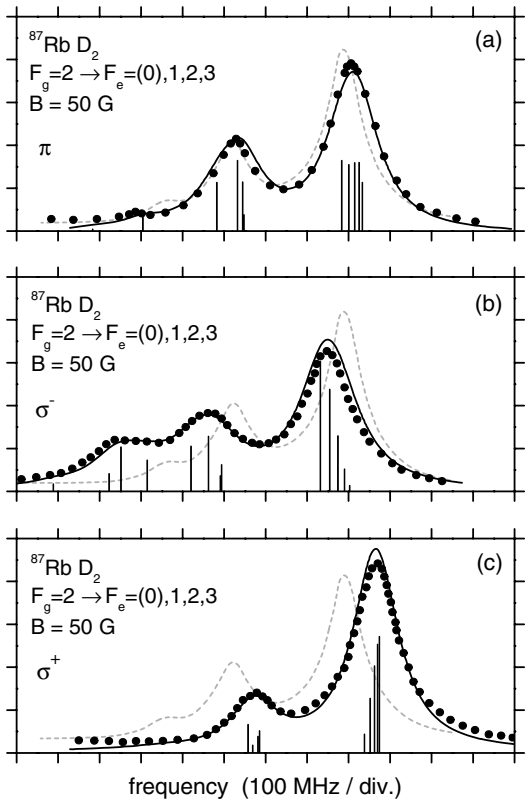


**Figure 9.** Experimental (scattered circles) and simulated (dark line) fluorescence spectra of $^{87}$Rb isotope on transitions $F_g = 2 \rightarrow F_e = 1, 2, 3, (4)$. (a) linearly polarized $\pi$ excitation, (b) circularly polarized $\sigma^-$ excitation, (c) circularly polarized $\sigma^+$ excitation. The respective fluorescence spectra in the absence of the magnetic field are shown with the light lines.

following model. We will assume that the laser radiation is weak and the absorption rate $\Gamma_p$ is small in comparison with the relaxation rates in the ground and excited states, denoted by $\gamma$ and $\Gamma$ respectively; $\Gamma_p < \gamma, \Gamma$. This assumption is well justified by the observation that the laser-induced fluorescence excitation spectrum is independent of the laser intensity.

The Hamiltonian operator of the atom in a magnetic field can be written as

$$\hat{H} = \hat{H}_0 + \hat{H}_{\mathrm{HFS}} - \boldsymbol{\mu}_J \cdot \mathbf{B} - \boldsymbol{\mu}_I \cdot \mathbf{B} \tag{1}$$

where $\hat{H}_0$ is the Hamiltonian operator of the unperturbed atom without taking into account nuclear spin, and $\hat{H}_{\mathrm{HFS}}$ represents hyperfine interaction. The remaining two terms represent the interaction of the electronic magnetic moment $\mu_J$ of the atom and the nuclear magnetic moment $\mu_I$ with the external magnetic field **B**. These magnetic moments are connected with the respective electronic and spin angular moments **J** and **I** of the atom

$$\boldsymbol{\mu}_J = -\frac{g_J \mu_{\mathrm{B}}}{\hbar}\mathbf{J}, \qquad \boldsymbol{\mu}_I = -\frac{g_I \mu_0}{\hbar}\mathbf{I}, \tag{2}$$

where $\mu_{\mathrm{B}}$ and $\mu_0$ are the Bohr and nuclear magnetons respectively and $g_J$, $g_I$ are electronic and nuclear Landé factors. The action of the magnetic field on the atom has two closely related effects. First, magnetic sublevels of the hyperfine levels are mixed by the magnetic field:

$$\begin{aligned} |\gamma_k m\rangle &= \sum_{F_{\mathrm{e}}=1-J_{\mathrm{e}}}^{F_{\mathrm{e}}=1+J_{\mathrm{e}}} C^{(\mathrm{e})}_{kF_{\mathrm{e}}}(B, m)|F_{\mathrm{e}}, m\rangle, \\ |\eta_j \mu\rangle &= \sum_{F_{\mathrm{g}}=1-J_{\mathrm{g}}}^{F_{\mathrm{g}}=1+J_{\mathrm{g}}} C^{(\mathrm{g})}_{jF_{\mathrm{g}}}(B, \mu)|F_{\mathrm{g}}, \mu\rangle, \end{aligned} \tag{3}$$

where $C^{(\mathrm{e})}_{kF_{\mathrm{e}}}(B, m)$ and $C^{(\mathrm{g})}_{jF_{\mathrm{g}}}(B, \mu)$ are mixing coefficients that depend on the field strength and magnetic quantum number $m$ or $\mu$. The second effect is deviation of the Zeeman magnetic sublevel splitting in the magnetic field for each hyperfine level from the linear one. This means that the additional energy of the magnetic sublevel obtained in the magnetic field is no longer linearly proportional to the field strength. New atomic states $|\gamma_k m\rangle$ and $|\eta_j \mu\rangle$ in the magnetic field in a general case are a linear combination of all initial hyperfine levels (four in the case of Rb atoms in the $5P_{3/2}$ state and two in the case of Rb atom in the $5S_{1/2}$ state). As is seen from equation (3), in the magnetic field the hyperfine angular momentum quantum number $F$ ceases to be a good quantum number, but the magnetic quantum numbers $m$ and $\mu$ are still good quantum numbers. This reflects the symmetry of the perturbation imposed by the magnetic field and means that only hyperfine sublevels with the same magnetic quantum numbers are mixed by the magnetic field.

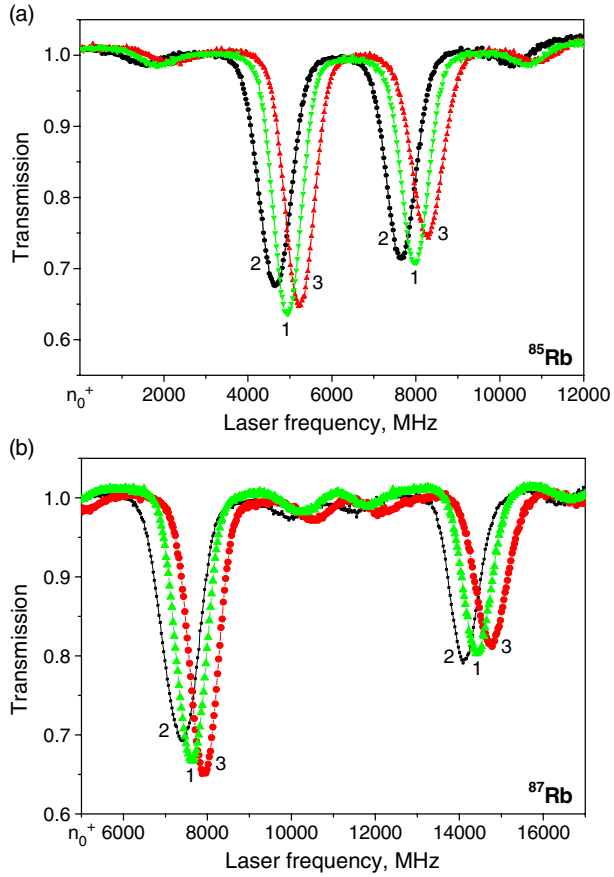


**Figure 10.** Absorption spectra in an ordinary optical cell for (a) $^{85}$Rb and (b) $^{87}$Rb. Peak 1 is absorption for $\sigma^-$ or $\sigma^+$ radiation in the absence of the magnetic field. Peak 2 corresponds to the absorption of $\sigma^-$ radiation in a magnetic field and peak 3 to the absorption of $\sigma^+$ radiation.

(This figure is in colour only in the electronic version)

The mixing coefficients $C^{(\mathrm{e})}_{k F_\mathrm{e}}(B, m)$ and $C^{(\mathrm{g})}_{j F_\mathrm{g}}(B, \mu)$ of the hyperfine states in the magnetic field and energies of these levels in the field ${}^{\gamma_k}E_m$, ${}^{\eta_j}E_\mu$ can be found as eigenvectors and eigenvalues of the Hamiltonian matrix (1). In figures 2 and 3 the energy levels obtained by the Hamiltonian matrix diagonalization for two Rb atom isotopes in the excited $5P_{3/2}$ state in the magnetic field are presented.

For Rb atoms in the ground state, hyperfine level splitting is larger than in an excited state. It is around 3 or 7 GHz for the two $^{85}$Rb and $^{87}$Rb isotopes respectively (see figure 4), which in both cases is large in comparison to the magnetic sublevel splittings obtained in the magnetic field of 50 G. As a result, ground state energy levels in the magnetic field can, to a very good level of approximation, be represented by the linear Zeeman effect, namely, ${}^{\eta_j}E_\mu = g_{\eta_j}\mu_\mathrm{B}B\mu/\hbar$, where $g_{\eta_j}$ is the Landé factor of the respective hyperfine level. For very weakly mixed levels it still can be represented with the hyperfine quantum number $F_\mathrm{g}$. For $^{85}$Rb atoms in the $5S_{1/2}$ state we have $g_{\eta_j} = -1/3$ for $F_\mathrm{g} = 2$ and $g_{\eta_j} = 1/3$ for $F_\mathrm{g} = 3$, and for $^{87}$Rb in the $5S_{1/2}$ state we have $g_{\eta_j} = -1/2$ for $F_\mathrm{g} = 1$ and $g_{\eta_j} = 1/2$ for $F_\mathrm{g} = 2$. In the case of mixing of only two hyperfine levels, the Breit–Rabi formula can be used to find both mixing coefficients and level energies (see, for example [36, 37]).

In the magnetic field, the excited state density matrix created by the laser light can be written as (see, for example [38])

$$ {}^{kl}f_{mm'} = \frac{\tilde{\Gamma}_p}{\Gamma + \mathrm{i}\,{}^{kl}\Delta\omega_{mm'}} \times \sum_{j\mu} \langle \gamma_k m|\hat{\mathbf{E}}^*_\mathrm{exc}\cdot\hat{\mathbf{D}}|\eta_j\mu\rangle\langle\gamma_l m'|\hat{\mathbf{E}}^*_\mathrm{exc}\cdot\hat{\mathbf{D}}|\eta_j\mu\rangle^*, \tag{4}$$

with ${}^{kl}\Delta\omega_{mm'} = ({}^{\gamma_k}E_m - {}^{\gamma_l}E_{m'})/\hbar$ being the energy splitting of the magnetic sublevels $m$ and $m'$ belonging to the excited state levels $k$ and $l$. The magnetic quantum numbers of the ground state level $\eta_j$ are denoted by $\mu$ and the magnetic quantum numbers of the excited state level $\gamma_{k,l}$ by $m$ and $m'$. In this last expression it is assumed that two magnetic sublevels of the excited state, that initially belonged to two different hyperfine levels at some specific magnetic field strength, can have the same energy and can be excited simultaneously and coherently. This means that nonzero field level crossing signals [38] in general can be included in this model. At the same time for practical calculations performed in this work this is not important, insofar as the laser radiation used to excite atoms in this work is chosen in such a way that it can be represented only by one component in a cyclic system of coordinates and is not able to create coherence between magnetic sublevels of the atom.

In our particular simulation we assume that, when we scan the laser frequency, only those transitions that are in an exact resonance with the laser field are excited. So at each laser frequency a specific density matrix is calculated. This density matrix is of course dependent on the magnetic field strength that determines the magnetic sublevel splitting and wavefunction mixing. The intensity of the fluorescence with a specific polarization $\mathbf{E}_\mathrm{obs}$ in a transition between the excited $\gamma_k$ and final $\eta_j$ state in the magnetic field can be calculated according to [38]

$$ I(\mathbf{E}_\mathrm{f}) = I_0 \sum_{mm'\mu}\sum_{klj} \langle\gamma_k m|\hat{\mathbf{E}}^*_\mathrm{obs}\cdot\hat{\mathbf{D}}|\eta_j\mu\rangle \times \langle\gamma_l m'|\hat{\mathbf{E}}^*_\mathrm{obs}\cdot\hat{\mathbf{D}}|\eta_j\mu\rangle^{*kl} f_{mm'}. \tag{5}$$

The final state of the transition may or may not coincide with the atomic hyperfine ground state level from which the absorption started. When in expressions for excited state density matrix elements (equation (4)) and fluorescence intensity (equation (5)) ground $|\gamma_k m\rangle$ and excited state $|\eta_j\mu\rangle$ wavefunction expansion over the atomic wavefunctions in absence of magnetic field is used (see equation (3)), matrix elements of the type $\langle F_\mathrm{e} m|\hat{\mathbf{E}}^*_\mathrm{exc}\cdot\hat{\mathbf{d}}|F_\mathrm{g}\mu\rangle$ appear. Standard methods of angular momentum theory can be used to calculate these matrix elements; see for example [32–35].

## 5. Analysis

For laser-induced fluorescence excitation spectra simulation in a magnetic field we use the following procedure. From the magnetic sublevel energy spectra obtained from the Hamiltonian matrix diagonalization we calculate the absorption line positions in a magnetic field. Then we calculate the absorption line strengths for these transitions, taking into account level mixing, the specific laser radiation polarization, and the magnetic field value. Then we assume

that the predominant factor in the formation of the absorption line shape is homogeneous broadening. In the general case the profile is a Voigt contour, which is a convolution of homogeneous (Lorentzian) and inhomogeneous (Gaussian) line shapes [39]. Our assumption that inhomogeneous broadening is substantially reduced in a sub-micron cell allows us to employ a Lorentzian absorption profile. From the energy levels, intensities, and line profiles we are able to create spectra of expected fluorescence intensity in the absence of spectral and polarization discrimination, but with specific emission directions. This means that in this way we are simulating laser-induced fluorescence excitation spectra for our excitation–observation conditions.

In figures 6–9, calculated intensities of fluorescence are shown as vertical bars of heights that represent the intensity of the fluorescence at a specific laser excitation frequency. Solid curves in the figures show laser-induced fluorescence excitation spectra that take into account the linewidth of each absorption line as described above. To get the best coincidence between measured and calculated spectra the homogeneous linewidth of each absorption component was assumed to be equal to 45 MHz. This is several times the natural linewidth of the resonant transition of the unperturbed Rb atom. The radiation width of the absorption components in $D_2$ line are expected to be approximately $\Delta\nu_{D_2} = 1/(2\pi\tau) \approx$ 6 MHz [31], where $\tau \approx 26$ ns is the lifetime of Rb in the $5P_{3/2}$ state. This absorption line broadening is partially due to the fact that we have a broad laser line—25 MHz. The rest of the broadening of the absorption line most probably can be attributed to the residual power broadening, residual Doppler broadening in the sub-micron cell and atomic collisions within the cell walls.

As can be seen from figures 6, 7, there is a remarkably good agreement between all measured signals and simulated laser-induced fluorescence excitation spectra for $^{85}$Rb isotopes. At the same time the agreement for the $^{87}$Rb isotope (figures 8, 9) in some cases could be better. We believe that these differences are caused by difficulties in experimental measurements. In our experiment the vapour density of the $^{87}$Rb isotope was approximately three times lower than the vapour density of the $^{85}$Rb isotope. As a result the signal from the $^{87}$Rb isotope was weaker and the spectra were measured with lower accuracy.

## 6. Conclusions

For the first time it was demonstrated that ETC can be successfully used to study spectra with sub-Doppler resolution of alkali atoms in a magnetic field. In particular, for a rather weak magnetic field of 50 G, when nuclear spin angular momentum **I** and electronic angular momentum **J** are only partially decoupled, we registered changes in laser-induced fluorescence excitation spectrum with sub-Doppler resolution of Rb atoms, when different polarizations of excitation laser were used. It was demonstrated that the spectra, when right- and left-hand circularly polarized excitation is used, differ very strongly and these differences are not only quantitative, but also qualitative. A strong magnetic field induced circular dichroism is clearly observed in this experiment.

On the one hand, it is not easy to characterize the difference in the shape of the laser-induced fluorescence excitation spectra in a quantitative way for different excitation light polarizations caused by a magnetic field. On the other hand, figures 6–9 clearly demonstrate this difference. Nevertheless, to give a quantitative idea about the magnitude of the magnetic field induced circular dichroism effect we can calculate the magnetic field induced difference in a total intensity of laser-induced fluorescence for left- and right-handed circularly polarized excitation. In the absence of the magnetic field, from a simple symmetry consideration it is obvious that these total intensities are equal for both circularities of the excitation radiation. When absorption takes place from the lower ground state hyperfine component with a smaller quantum number $F_g$, the magnetic field increases the total absorption for the $\sigma^+$ polarized light. This increase in comparison to the total intensity produced by a $\sigma^-$ radiation in our calculation for magnetic field strength 50 G can reach more than 20% (figure 6). For absorption from the upper ground state hyperfine component $F_g$ the effect is the opposite, and a decrease of the total laser-induced fluorescence intensity for $\sigma^+$ excitation in comparison to $\sigma^-$ excitation can be more than 6% (figure 7).

The appearance of this circular dichroism may be explained in a standard approach, which describes how partial decoupling of **I** and **J** mixes together magnetic sublevels of different hyperfine states of alkali atoms. As a result, we have a nonlinear Zeeman effect for each magnetic sublevel. A second consequence of this mixing of wavefunctions of different hyperfine states is a substantial modification of transition probabilities between different magnetic sublevels, including the fact that transitions that are strictly forbidden in the absence of the magnetic field start to be allowed. These effects of quantum state mixing in the presence of the external magnetic field play an important role also in a level crossing spectroscopy; see for example [36, 40, 41]. The importance of these changes of transition probabilities even for the case of a rather weak magnetic field illustrates that thin cells can show a sensitivity to physical processes not accessible to conventional Doppler-broadened spectroscopy.

## Acknowledgments

The authors are very thankful to Professor Neil Shafer-Ray for fruitful discussions. The authors are grateful to A Sarkisyan for his valuable participation in the fabrication of the ETC. This work was supported, in part, by ANSEF Grant No PS 18-01 and Armenian Republic Grants No 1351, 1323.

## References

[1] Schawlow A L 1982 *Rev. Mod. Phys.* **54** 697
[2] Letokhov V S and Chebotayev V P 1977 *Nonlinear Laser Spectroscopy* (*Springer Series in Optical Sciences* vol 4) (Berlin: Springer)
[3] Wynands R and Nage A 1999 *Appl. Phys.* B **68** 1
[4] Glassner D S, Ai B and Knize R J 1994 *Opt. Lett.* **19** 2071
[5] Ai B, Glassner D S, Knize R J and Partanen J P 1994 *Appl. Phys. Lett.* **64** 951
[6] Briaudeau S, Bloch D and Ducloy M 1996 *Europhys. Lett.* **35** 337
[7] Briaudeau S, Saltiel S, Nienhuis G, Bloch D and Ducloy M 1998 *Phys. Rev.* A **57** R3169

[8] Briaudeau S, Bloch D and Ducloy M 1999 *Phys. Rev.* A **59** 3723
[9] Briaudeau S, Saltiel S, Leite J R R, Oria M, Bramati A, Weis A, Bloch D and Ducloy M 2000 *J. Physique* **10** Pr8-145
[10] Izmailov A 1993 *Laser Phys.* **3** 507
[11] Romer R H and Dicke R H 1955 *Phys. Rev.* **99** 532
[12] Vartanyan T A and Lin D L 1995 *Phys. Rev.* A **38** 5197
[13] Zambon B and Nienhuis G 1997 *Opt. Commun.* **143** 308
[14] Dutier G, Yarovitski A, Saltiel S, Papoyan A, Sarkisyan D, Bloch D and Ducloy M 2003 *Europhys. Lett.* **63** 35
[15] Dutier G, Saltiel S, Bloch D and Ducloy M 2003 *J. Opt. Soc. Am.* B **20** 793
[16] Sarkisyan D, Bloch D, Papoyan A and Ducloy M 2001 *Opt. Commun.* **200** 201
[17] Khriplovich I B and Lamoreaux S K 1997 *CP Violation Without Strangeness, Electric Dipole Moments of Particles, Atoms, and Molecules* (Berlin: Springer)
[18] Commins E D 1993 *Phys. Scr.* **46** 92
[19] Bouchiat M A and Bouchiat C 1997 *Rep. Prog. Phys.* **60** 1351
[20] Guena J, Chauvat D, Jacquier Ph, Jahier E, Lintz M, Sanguinetti S, Wasan A, Bouchiat M A, Papoyan A V and Sarkisyan D 2003 *Phys. Rev. Lett.* **90** 143001
[21] Wood C S, Bennett S C, Cho D, Masterson B P, Roberts J L, Tanner C E and Wieman C E 1997 *Science* **275** 1759
[22] Yashchuk V V, Budker D and Davis J R 2000 *Rev. Sci. Instrum.* **71** 341
[23] Clifford M A, Lancaster G P T, Conroy R S and Dholakia K 2000 *J. Mod. Opt.* **47** 1933
[24] Corwin K L, Lu Z T, Hand C F, Epstein R J and Wieman C E 1998 *Appl. Opt.* **37** 3295
[25] Novikov V N, Sushkov O P and Khriplovich I B 1977 *Opt. Spectrosc.* **42** 370
Novikov V N, Sushkov O P and Khriplovich I B 1978 *Opt. Spectrosc.* **45** 236
[26] Roberts G J, Baird P E G, Brimicombe M W S, Sandars P G H, Selby D R and Stacey D N 1980 *J. Phys. B: At. Mol. Phys.* **13** 1389
[27] Chen X, Telegdi V L and Weis A 1987 *J. Phys. B: At. Mol. Phys.* **20** 5653
[28] Tremblay P, Michaud A, Levesque M, Theriault S, Breton M, Beaubien J and Cyr N 1990 *Phys. Rev.* A **42** 2766
[29] Weis A, Sautenkov V A and Hansch T W 1993 *J. Physique* **3** 263
[30] Papageorgiou N, Weis A, Sautenkov V A, Bloch D and Ducloy M 1994 *Appl. Phys.* B **59** 123
[31] Theodosiou C E 1984 *Phys. Rev.* A **30** 2881
[32] Auzinsh M and Ferber R 1995 *Optical Polarization of Molecules* (Cambridge: Cambridge University Press)
[33] Zare R N 1988 *Angular Momentum* (New York: Wiley)
[34] Varshalovich D A, Moskalev A N and Khersonskii V K 1988 *Quantum Theory of Angular Momentum* (Singapore: World Scientific)
[35] Sobelman I I 1979 *Atomic Spectra and Radiative Transitions* (Berlin: Springer)
[36] Aleksandrov E B, Chaika M P and Khvostenko G I 1993 *Interference of Atomic States* (New York: Springer)
[37] Svanberg S 1992 *Atomic and Molecular Spectroscopy: Basic Aspects and Practical Applications* (Berlin: Springer)
[38] Alnis J and Auzinsh M 2001 *Phys. Rev.* A **63** 023407
[39] Demtroder W 2002 *Laser Spectroscopy: Basic Concepts and Instrumentation* (Berlin: Springer)
[40] Aleksandrov E B 1972 *Sov. Phys.—Usp.* **15** 436
[41] Series G W 1981 *Contemp. Phys.* **22** 487